Disorder and double-exchange spin dynamics in $La_{0.7}Sr_{0.3}MnO_3$ and $La_{0.7}Sr_{0.3}CoO_3$ from NMR hyperfine couplings

M. J. R. Hoch,[1] P. L. Kuhns,[1] W. G. Moulton,[1] A. P. Reyes,[1] M. A. Torija,[2] J. F. Mitchell,[3] and C. Leighton[2]
[1]*National High Magnetic Field Laboratory, Florida State University, 1800 East Paul Dirac Drive, Tallahassee, Florida 32310, USA*
[2]*Department of Chemical Engineering and Materials Science, University of Minnesota, Minneapolis, Minnesota 55455, USA*
[3]*Materials Science Division, Argonne National Laboratory, Argonne, Illinois 60439, USA*
(Received 12 December 2006; published 26 March 2007)

The hole-doped transition metal oxides $La_{1-x}Sr_xMnO_3$ (LSMO) and $La_{1-x}Sr_xCoO_3$ (LSCO) show certain similarities to each other in their physical properties but also marked differences. In the metallic-ferromagnetic doping range, important properties of these materials, such as nanoscale phase separation, are due to competing double-exchange ordering interactions and disordering Jahn-Teller (JT) distortions. The present experiments have used low magnetic field NMR of the ^{55}Mn and ^{59}Co transition metal ion nuclei in $x=0.3$ samples to obtain information on changes in hyperfine couplings and spin dynamics as a function of temperature. At low temperatures, anisotropy effects linked to lattice distortions are more important in LSCO than in LSMO. Structural distortions become important in LSMO above 120 K.

DOI: 10.1103/PhysRevB.75.104421 PACS number(s): 75.30.−m, 72.25.Ba, 76.60.Jx

INTRODUCTION

The transition metal oxides, such as $La_{1-x}Sr_xMnO_3$ (LSMO) and $La_{1-x}Sr_xCoO_3$ (LSCO), are of particular interest because of the large magnetoresistance (MR) properties they exhibit and the theoretical challenges they pose.[1–5] Considerable evidence has been obtained that in both systems nanoscale phase separation is important.[4–8] This phenomenon is due to competition between ordering and disordering interactions that are comparable in strength.

Ferromagnetism (FM) in mixed valence LSMO and LSCO is a result of the double-exchange (DE) mechanism.[9–11] The process involves electron transfer, via an oxygen intermediary, between octahedrally coordinated transition metal ions in different charge states. DE plays a key role in determining many of the properties of these oxide systems such as nanoscale phase separation and the large MR. While considerable theoretical effort has been made to model LSMO in order to understand its properties,[4,12–14] less effort has been devoted to modeling LSCO. This is due, at least partly, to the complicating effects associated with the spin state transition that is known to occur in $LaCoO_3$ (LCO).

While there are some similarities in the phase diagrams of LSMO (Ref. 15) and LSCO,[7] there are important differences. For $x\sim0.18$, both systems exhibit a metal-insulator (MI) transition to a FM metallic phase at low temperatures. However, LSMO exhibits antiferromagnetism (AFM) for $x<0.18$, while LSCO has a spin glass or cluster glass phase in this range. There are further differences related to charge ordering and orbital ordering which become important in LSMO as x is increased towards 0.5. For $x\sim0.3$, the crystal structures for both systems are rhombohedral corresponding to a small distortion from cubic symmetry. For the undoped systems, the energy gap between the t_{2g} and e_g levels is ~1 eV in $LaMnO_3$ (Ref. 2) and is much smaller ~10 meV in $LaCoO_3$.[16] In the latter case, thermally activated spin state conversion from low-T, low-spin [(LS); $S=0$] to intermediate spin [(IS); $S=1$] occurs as T is raised. For the hole-doped LSCO system, the IS state appears to be stabilized over spatially extended regions at low T for $x>0.05$.[5,17] In both LSMO and LSCO, Hund's rule exchange coupling of the electron in the e_g state to the core localized spins in the t_{2g} levels is important with this coupling stronger to the core spins in LSMO, which has half-filled t_{2g} states, than in LSCO. The small gap in $LaCoO_3$ is due to the competing effects of crystal field splitting of the levels and the Hund's rule coupling.[16] It is interesting to note that the tolerance factor,[2] involving the ionic radii, is slightly closer to unity for $LaCoO_3$ (LS and IS) than it is for $LaMnO_3$ but that lattice distortions appear to be more important at low T in LSCO than in LSMO, as discussed below.

Considerable evidence exists that the intrinsic phase separation found in the manganites is primarily due to competition between the delocalizing effects of DE and the localizing effects of Jahn-Teller (JT) distortions or other disorder.[12–14] It is likely that static and/or dynamic JT distortions play a role in phase separation in the cobaltites but further work is needed to confirm this. Recent experiments have shown that the nanoscale phase separation is different in single crystal LSCO than in high quality sintered samples, occurring over a narrower range of x values on either side of the MI transition in single crystals.[18] This has in part motivated the present experiments on single crystal LSCO. In view of the importance of the DE mechanism in understanding LSMO and LSCO, it is desirable that information on spin dynamics be obtained using microscopic techniques. The present work has sought to compare DE related phenomena in LSMO and LSCO, and in particular the evolution with T of this interaction using FM NMR.

EXPERIMENTAL

Sintered powder samples of LSMO and LSCO with $x=0.3$ were prepared by solid state reaction at high temperature.[7] In addition, a single crystal of LSCO with $x=0.30$ was grown using floating zone methods.[18] The samples were characterized by x-ray and neutron diffraction,

 ©2007 The American Physical Society

thermogravimetric analysis and energy dispersive spectroscopy in a scanning electron microscope. Electrical resistivity measurements were made on the samples as a function of T. The single crystal sample of LSCO was crushed for the NMR experiments to overcome skin-depth effects and permit rf penetration into the metallic grains.

The zero-field (ZF) and low-field NMR experiments were carried out using a pulsed NMR spectrometer with a frequency calibrated, untuned, variable temperature probe. Spectra were obtained by stepping the frequency and recording spin echo signal amplitudes. ^{55}Mn and ^{59}Co spin-spin $W_2=1/T_2$, and spin-lattice $W_1=1/T_1$, relaxation rate measurements used spin echo and saturation recovery methods, respectively. Magnetic fields of a few T could be applied to the samples using a superconducting solenoid in order to magnetize the sample and sweep out domain walls, thus avoiding complications in analysis of the data due to mixed contributions from domains and walls.

NUCLEAR RELAXATION IN DOUBLE-EXCHANGE SYSTEMS

DE oxides represent a special class of itinerant FMs. In this section we summarize the available theoretical expressions for nuclear spin-lattice and spin-spin relaxation in FM systems that are used in the analysis of our data. In addition, a phenomenological approach that includes changes in the hyperfine anisotropy of these systems with temperature is presented.

The Hamiltonian for e_g electrons undergoing DE and interacting with core t_{2g} spins is written as[3]

$$H=\sum_{i,j,\sigma} t_{ij}c_{i\sigma}^{\dagger}c_{j\sigma}-J_H\sum_{i,\sigma,\sigma'}(\boldsymbol{S}_i\cdot\boldsymbol{\sigma}_{\sigma,\sigma'})c_{i\sigma}^{\dagger}c_{i\sigma'}, \tag{1}$$

where t_{ij} is the transfer integral, $c_{i\sigma}^{\dagger}$ and $c_{j\sigma}$ are creation and annihilation operators for an electron with spin σ at nearest neighbor sites i and j, respectively, J_H is the Hund's rule coupling and, in general, $J_H>t_{ij}$. σ is the Pauli spin matrix. The transfer integral depends on the angle θ between the core spins S_i and S_j and is given by $t_{ij}=t_m\cos(\theta/2)$, where t_m is the maximum value that t_{ij} takes. Systems in which Eq. (1) applies, such as LSMO and LSCO, behave as highly spin-polarized FM conductors for $T\ll T_C$.

Expressions for the nuclear spin-lattice relaxation and spin-spin relaxation rates W_1 and W_2 may be obtained in the low-T case ($T\ll T_C$) by adapting the formalism for nuclear relaxation in d-band FM metals that allows for the symmetry of the conduction electron wave functions.[19–21] Conduction electron contributions to the relaxation rate W_1 include orbital, dipolar, and core polarization (CP) terms $W_1=W_1^{\mathrm{orb}}+W_1^{\mathrm{dip}}+W_1^{\mathrm{CP}}$. Phonon-mediated quadrupolar relaxation contributions are generally assumed negligible in itinerant FMs, but spin wave relaxation may be important in some cases and, as we shall see, is the dominant mechanism at low T in LSMO. In FM such as metallic Co, the orbital contribution may be written in the tight binding approximation as[20]

$$\frac{W_1^{\mathrm{orb}}}{T}=(16\pi/5)\gamma_I^2\hbar k_B\langle H_{\mathrm{hf}}^{\mathrm{orb}}\rangle_F^2[\rho_{\downarrow}^2(E_F)+\rho_{\uparrow}^2(E_F)]F^{\mathrm{orb}}(\Gamma), \tag{2}$$

with γ_I the nuclear gyromagnetic ratio, $\langle H_{\mathrm{hf}}^{\mathrm{orb}}\rangle_F$ the d-electron orbital field averaged over the Fermi surface, $\rho_{\downarrow(\uparrow)}^2(E_F)$ the square of the spin down (up) density of d-band states for spins at the Fermi level. For DE systems with large spin polarizations we expect that one spin band is primarily responsible for nuclear relaxation. W_1^{orb} depends on the atomic d-electron wave functions used in constructing the Bloch functions through the function $F^{\mathrm{orb}}(\Gamma)=[1-(C-1)^2]$ where the parameter C measures the admixture of $t_{2g}(\Gamma_5)$ orbitals at the Fermi surface. For equal weights (1/5 each) of the three t_{2g} and two e_g orbitals we obtain $C=1$, and it follows that $F^{\mathrm{orb}}(\Gamma)=1$ while $F^{\mathrm{orb}}(\Gamma)<1$ for smaller values of C.

We now consider the possible contribution to nuclear relaxation in these DE oxides due to the dipolar mechanism and briefly consider the core polarization mechanism. For FM transition metals these contributions to relaxation are much smaller than the orbital contribution.[20] In the oxides it is not possible to separate contributions from the various mechanisms with any certainty in view of the lack of detailed knowledge of the $t_{2g}(\Gamma_5)$ character of the wave functions at the Fermi surface mentioned above. Adapting the Moriya approach,[20] the relaxation rate expression for this process is similar to Eq. (1), and the ratio of the orb and dip relaxation rates may be written as

$$\frac{W_1^{\mathrm{dip}}}{W_1^{\mathrm{orb}}}\approx\frac{\langle H_{\mathrm{hf}}^{\mathrm{dip}}\rangle^2}{\langle H_{\mathrm{hf}}^{\mathrm{orb}}\rangle^2}\left[\frac{F^{\mathrm{dip}}(\Gamma)}{F^{\mathrm{orb}}(\Gamma)}\right], \tag{3}$$

with $\langle H_{\mathrm{hf}}^{\mathrm{dip}}\rangle_F$ the hyperfine field due to dipolar coupling. Calculations show that $F^{\mathrm{dip}}(\Gamma)<F^{\mathrm{orb}}(\Gamma)$ except when C tends to zero.[19,20] W_1^{dip} may play a minor role in nuclear relaxation in LSCO and LSMO depending on the $F^{\mathrm{dip}}(\Gamma)/F^{\mathrm{orb}}(\Gamma)$ ratio. Band theory calculations are needed to in order to determine the relative importance of the orbital and dipolar contributions to relaxation in these systems. The core polarization contribution in transition metals has been considered by Yafet and Jaccarino[21] and in FM transition metals by Moriya[20] and is shown to be small compared to the orbital contribution. Based on the Moriya estimate, we assume that core polarization relaxation may be neglected in the DE oxides.

At low T, spin wave contributions to nuclear relaxation need to be considered. In the case of a noncubic lattice where the hyperfine interaction is not isotropic, the electron (S) and nuclear (I) spins are in general quantized along different directions z and z', respectively, and we write the perturbing hyperfine Hamiltonian as

$$H_{\mathrm{hf}}=A_1I_{x'}(S_x\cos\alpha+S_z\sin\alpha)+A_2I_{y'}S_y+A_3I_{z'}(S_z\cos\alpha-S_x\sin\alpha), \tag{4}$$

where α is the angle between z and z' with y and y' chosen to coincide. The A_i are the principal values of the hyperfine coupling tensor. Fluctuations in the A_i or the S_j lead to

nuclear relaxation. Expressions for W_1 as a function of T for various magnon processes have been obtained using time dependent perturbation theory.[22,23] The magnon dispersion relation for a FM in a field H has the form $E_k \approx g\mu_B SH + 2JSka^2$, where J is the exchange coupling, μ_B the Bohr magneton, and a the lattice spacing. In single magnon nuclear relaxation processes small k excitations are important. An applied field produces a gap at $k=0$ which reduces the effectiveness of such processes and higher order mechanisms such as two and three magnon processes or phonon-magnon processes need to be considered.[23] In general, these processes lead to a dependence on some power of T higher than unity.

Considering two-magnon processes[23] gives for $k_BT \ll 2JS$ and $k_BT \gg g\beta H$

$$W_1 = \frac{A^2(\sin^2\alpha)k_B}{2(2\pi)^3\hbar(2JS)^3}T^2\ln(k_BT/g\beta H). \quad (5)$$

In metallic FMs the Korringa relaxation mechanism is often dominant over the spin wave mechanism, but spin waves appear to be important in LSMO at low T.

At temperatures not much less than T_C, it is necessary to modify the relaxation expressions to allow for disorder effects such as JT distortions. It is not simple to allow for the resulting changes in the electronic structure in a quantitative way. Therefore, we adopt a phenomenological formalism by introducing a correlation time τ to describe the time dependence of fluctuating hyperfine fields. We note that previous phenomenological DE relaxation rate expressions used in analyzing data in manganites and cobaltites are of the form $W_1 = \langle H_{\rm hf}^2\rangle\tau$ with τ the electron correlation time assumed to be T dependent.[24,25] This approach is extended to give an expression for W_1, allowing for hyperfine anisotropy, and is cast in a form similar to Eq. (2).

The perturbing Hamiltonian given in Eq. (4) may be written in terms of raising and lowering operators as

$$H = \frac{1}{2}A_1(I_+ + I_-)\left[S_z\sin\alpha + \frac{1}{2}(S_+ + S_-)\cos\alpha\right] - \frac{1}{4}A_2(I_+ - I_-) \times (S_+ - S_-) + \frac{1}{2}A_3 I_{z'}\left[S_z\cos\alpha - \frac{1}{2}(S_+ + S_-)\sin\alpha\right]. \quad (6)$$

As a simplifying approximation, we disregard the spin-flip terms involving S_+ and S_- for the highly spin polarized DE system. (This may not be a good assumption at higher temperatures where spin-flip electron scattering processes might contribute to relaxation but the inclusion of small additional contributions will not change the relaxation expression significantly.) The perturbing Hamiltonian may be written as[26] $H = \Sigma_k L^k P^k$ with the lattice operators given by $L^0 = \frac{1}{2}A_3 S_z\cos\alpha$, $L^1 = \frac{1}{2}A_1 S_z\sin\alpha$ and the spin operators by $P^0 = I_{z'}$, $P^{\pm 1} = I_\pm$. Using the density matrix approach gives for the rate of change of the average nuclear magnetization operator $\langle I\rangle$ the general expression $\frac{d\langle \boldsymbol{I}\rangle}{dt} = -1/2\Sigma J_k(\omega_m^k) \times \{\langle [P_m^k,[P_m^{-k},\boldsymbol{I}]]\rangle - \langle\cdots\rangle_0\}$ where the spectral densities $J_k(\omega_m^k)$ are obtained as the Fourier transforms of the correlation functions[26]

$$G_0(\tau) = \frac{1}{3}\langle A_3(\tau)A_3(0)\rangle S(S+1)\cos^2\alpha, \quad (7)$$

$$G_\pm(\tau) = \frac{1}{3}\langle A_1(\tau)A_1(0)\rangle S(S+1)\sin^2\alpha. \quad (8)$$

The angular brackets represent an ensemble average. The relaxation rate is given by $\frac{d\langle I_z\rangle}{dt} = -W_1[\langle I_z\rangle - I_0]$, where I_0 is the thermal equilibrium value of I. In the short correlation time limit, using the x and y components of I and taking into account that only carriers with energy close to the Fermi energy $E_F = k_BT_F$ can participate in relaxation gives

$$W_1 = \frac{2}{3}S(S+1)(T/T_F)[A_1^2\sin^2\alpha]\tau. \quad (9)$$

τ is the correlation time for the hyperfine fluctuations, and we assume that the correlation function decays rapidly with time. At low temperatures, in the good metal limit, we can take $\tau = \tau_0 \approx \hbar/E_F$ and rearranging Eq. (9) we obtain $W_1 \approx \frac{2}{3}S(S+1)\hbar k_BT/E_F^2[A_1^2\sin^2\alpha]$. Since $\rho(E_F) \sim N/E_F$ it follows that at low T the form of Eq. (9) is similar to that of Eq. (2). If JT distortions become important with increasing T, changes in the character of the conduction band wave functions and in the anisotropy of $H_{\rm hf}$ will occur. In addition, the DE coupling will change as the core spins become less well ordered. We can allow for disordering using the transfer integral dependence on the core spin orientations θ, which suggests the simple form

$$\tau \sim \tau_0/\langle\cos(\theta/2)\rangle, \quad (10)$$

where the angular brackets indicate an ensemble average. For the DE oxides the bandwidth is given by $6t_m\cos(\theta/2)$. The bandwidth is reduced by disorder, and this leads to changes in the DOS and enhanced localization effects.[2] The phenomenological expression given in Eq. (9) captures changes in the electronic structure through the correlation time τ which is increased by disorder.

Finally, we note the relaxation rate prediction $W_2 \approx W_1$ in isotropic FM systems.[27] In the noncubic anisotropic case we note that $W_2 > W_1$, due to different secular and nonsecular contributions [corresponding to the correlation functions given in Eqs. (7) and (8) respectively] but that the two rates, which are proportional to τ, will have similar T dependences. Equations. (2), (3), (5), and (9) are used below in discussing the experimental results.

RESULTS AND DISCUSSION

A. Electrical resistivity

The electrical resistivity ρ values for single crystal $x = 0.3$ LSMO and LSCO samples are shown as a function of T in Fig. 1. The LSCO results are for the sample used in the present experiments while the LSMO data is taken, with permission of the authors, from Ref. 28. Resistivity measurements on the sintered LSMO sample, for which NMR results are presented below, show similar form to that for the single crystal but with higher resistivity values attributed to grain

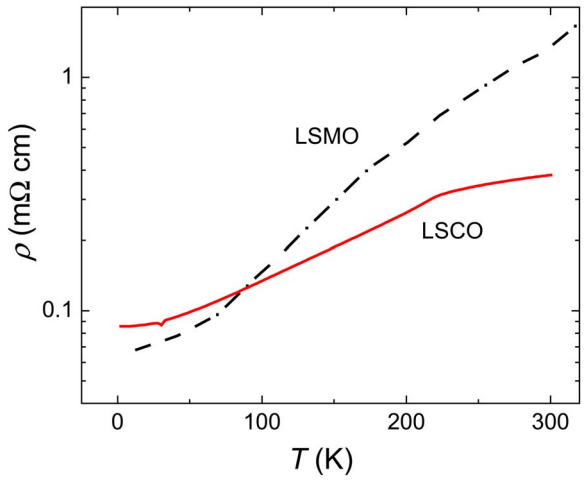

FIG. 1. (Color online) Electrical resistivity as a function of T for single crystal samples of $La_{0.7}Sr_{0.3}MnO_3$ and $La_{0.7}Sr_{0.3}CoO_3$. The LSMO data is taken from Ref. 27 (with permission of the authors).

boundary effects and the granular (lower density) nature of the sample. The granularity of the sample is not important in the NMR measurements because of the microscopic nature of the technique. Figure 1 shows that at 4 K LSMO is a slightly better conductor than LSCO but that the resistivity becomes larger than that of LSCO as T is raised to above 300 K, increasing by more than an order of magnitude over this range. For LSCO the increase is more gradual by a factor of roughly 3 between 4 and 300 K. It is well known that, in the vicinity of the Curie point, magnetoresistance effects, linked to spin dependent transport, are much larger in LSMO than in LSCO. The absence of magnetoresistance effects at low T in both samples suggests that magnetic disorder is not responsible for the residual resistance.

B. NMR spectra and relaxation rates

^{55}Mn NMR spectra for LSMO in an applied field of 3 T are shown as a function of T in Fig. 2. For LSCO, where there is little dependence of the broad spectrum on magnetic field or temperature, Fig. 3 shows a representative ^{59}Co LSCO spectrum in a field 0.5 T at 4 K. The FM NMR enhancement factors η[27] were roughly two orders of magnitude larger for LSMO than for LSCO and showed a much larger H dependence decreasing from $\eta \sim 10^4$ in ZF to $\eta \sim 10^2$ for $H > 1$ T, while for LSCO the corresponding decrease is a factor of 3 with $\eta \sim 70$ in ZF. The enhancement factor results show a large difference in magnetic anisotropy. For FM NMR, we have $\eta = H_{hf}/(H + H_{an})$, where H_{hf} is the hyperfine field at a nuclear site and H_{an} is the anisotropy field.[27] The observation that $\eta_{LSMO} \gg \eta_{LSCO}$ suggests that H_{an} is much smaller in LSMO than in LSCO. It is well known that η is significantly larger within domain walls than in bulk domain regions.[27] To avoid domain wall effects, the spectra were recorded and relaxation rates measured in saturating applied magnetic fields of 3.0 T for LSMO and 0.5 T for LSCO. The spectra for LSCO showed little change with increasing H but for LSMO the changes were significant with a high frequency shoulder diminishing with H until the line shape became a single Gaussian with a peak at f_{max}. The fields used correspond to values for which the spectral shapes were insensitive to changes and the magnetization curves are saturated. Previous FM NMR measurements on LSMO (Ref. 29) and LSCO (Refs. 8 and 30) were made in ZF.

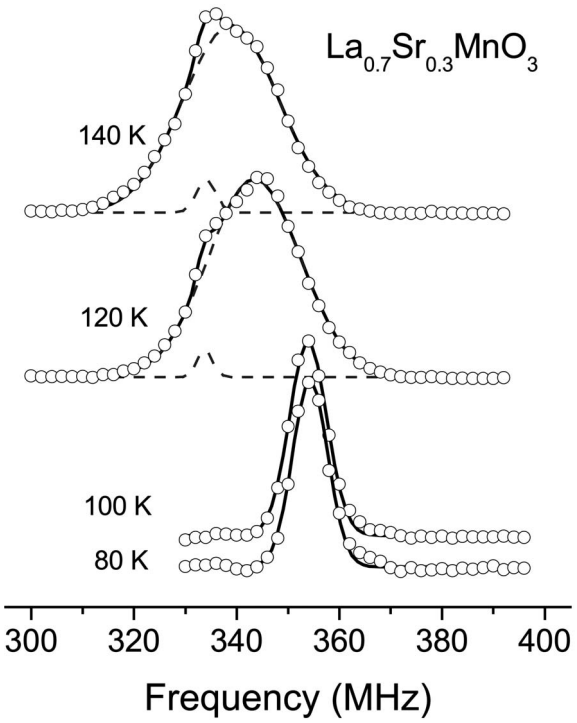

FIG. 2. ^{55}Mn FM-NMR spectra (with amplitudes in arbitrary units) for sintered $La_{0.7}Sr_{0.3}MnO_3$ as a function of T in an applied field of 3 T. Fitted Gaussians are shown as the full curves. Line shape changes are found for $T > 100$ K and the fitted spectra require two Gaussians with the two components shown as the dash curves. (The signal amplitudes decrease with rising T as expected. To facilitate comparison of the shapes the peak heights were adjusted to be approximately the same by changing the spectrometer gain.)

For LSCO, the reduced linewidth $\Delta f/f_{max} \sim 0.3$ and is independent of H. The relatively small reduced in-field linewidth in LSMO, $\Delta f/f_{max} \sim 0.02$ for $T < 100$ K, points to a smaller distribution of hyperfine fields than is found in LSCO. The domain wall thickness d in FM has the form $d \propto \sqrt{J/K}$, where K is the anisotropy constant and J the exchange coupling between neighboring spins. Taking $J^{LSMO} > J^{LSCO}$ and $K^{LSMO} \ll K^{LSCO}$, it follows that $d^{LSMO} \gg d^{LSCO}$ consistent with the present findings concerning η in the two systems. Nuclei in domain walls in LSCO, constituting a reduced fraction of the total in the sample, may be expected to make a smaller contribution to the ZF signal than the domain wall nuclei do in LSMO. This explains the small H dependence of the spectrum in LSCO. Summarizing, these observations based on the NMR spectra show that, in many respects, LSMO behaves similar to a conventional low anisotropy FM metal at low T, while LSCO behaves somewhat differently with the hyperfine and magnetic anisotropy effects being much larger than in LSMO.

Figure 4 shows the ^{55}Mn and ^{59}Co spin-lattice relaxation rates for the LSMO and LSCO samples as a function of $1/T$.

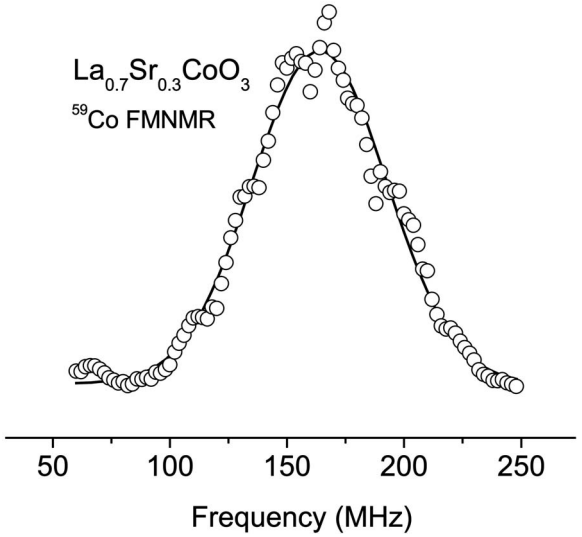

FIG. 3. ^{59}Co FM-NMR $T=2$ K spectrum for crushed single crystal $La_{0.7}Sr_{0.3}CoO_3$ in an applied field of 0.5 T. The amplitude is in arbitrary units. The line shape is robust and no changes were found with increasing T or H although the enhancement factor η decreased by a factor 3 with increasing H consistent with diminishing "domain wall" contributions. The single Gaussian fitted curve width is 57 MHz.

There have been few relaxation measurements made on the manganites, and these have been carried out in zero applied field. For LSCO previous ZF data for sintered $x=0.14$ and 0.4 samples[25] is shown for comparison and is in agreement with the single crystal values. (Note that there is a typographical error in the units on the y axis in Fig. 1 of Ref. 25. The units should be μ s^{-1} not s^{-1}.) W_1^{LSCO} is independent of frequency across the central portion of the spectrum. The contrast in behavior between LSMO and LSCO is striking

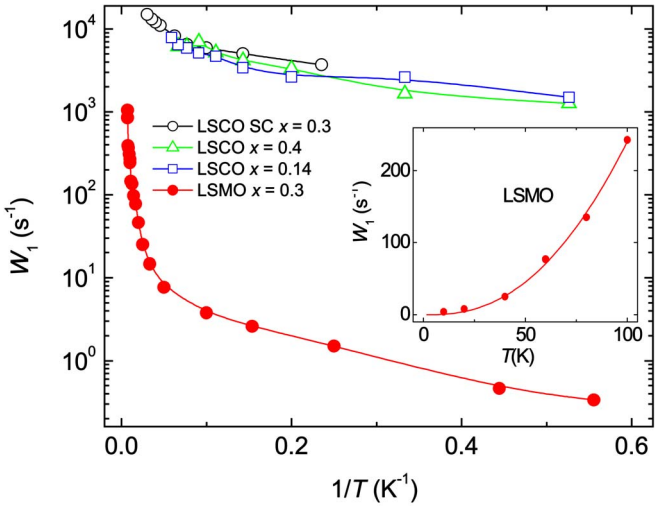

FIG. 4. (Color online) Relaxation rates for ^{55}Mn in $La_{0.7}Sr_{0.3}MnO_3$ and ^{59}Co in $La_{0.7}Sr_{0.3}CoO_3$ as a function of $1/T$. The additional LSCO data for $x=0.14$ and 0.4 (sintered samples) are from the zero-field results of Ref. 25. The inset shows the fit to the LSMO data based on a two-magnon mechanism for the temperature range 10–100 K. Details are given in the text.

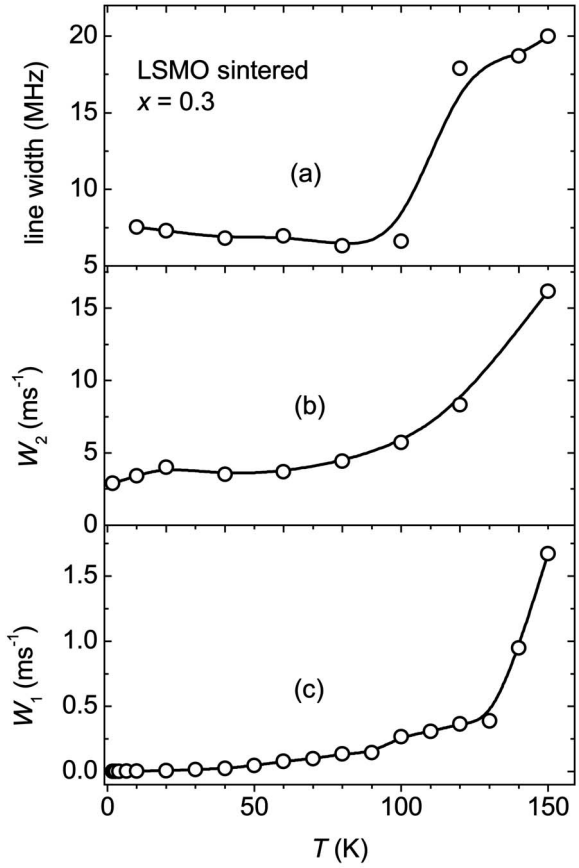

FIG. 5. ^{55}Mn FM-NMR parameters as a function of T for $La_{0.7}Sr_{0.3}MnO_3$ measured in an applied field of 3 T: (a) linewidth Δf, (b) spin-spin relaxation rate W_2, and (c) spin-lattice relaxation rate W_1.

with the relaxation rate ratio $W_1^{\mathrm{LSCO}}/W_1^{\mathrm{LSMO}} > 10^3$ at 4 K.

Plots of the linewidth Δf versus T and the relaxation rates W_2 and W_1, measured at the spectral center frequencies, versus T are shown for LSMO in Fig. 5 and for LSCO in Fig. 6. Within experimental uncertainty, the relaxation rates in LSMO are insensitive to frequency across the spectrum. Previous relaxation rate measurements on manganites and cobaltites were made in ZF, and in the case of $La_{1-x}Na_xMnO_3$ only for $T>60$ K.[24] The present in-field measurements remove domain wall contributions that can complicate analysis of the relaxation rate results. The spectra for LSCO show a negligible H dependence, other than a diminution in amplitude corresponding to the change in η. The results from the powder and single crystal samples are in good agreement and confirm the previous measurements,[25] despite the different phase separation characteristics of sintered and single crystal samples. It appears that the FM regions in LSCO are robust and not dependent on the method of preparation, or on x. While the data for LSCO extend over a much smaller temperature range than those for LSMO, Figs. 5 and 6 suggest that the ^{55}Mn and ^{59}Co W_1 and W_2 behaviors with T in the two systems are markedly different. The near-linear T dependence of $^{59}W_1$ in LSCO is contrasted with the nonlinear dependence of $^{55}W_1$ on T in LSMO. It should be noted that, while the relaxation rate variation with T in LSCO is

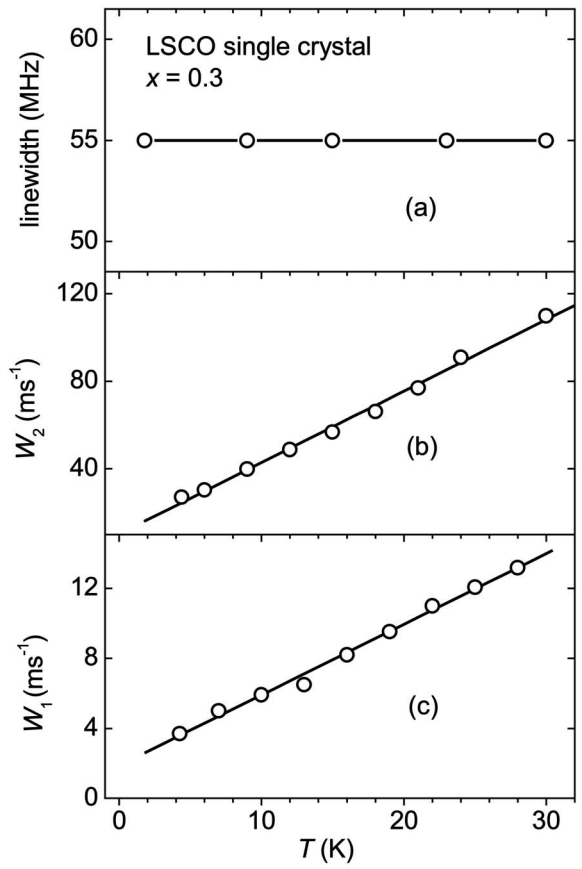

FIG. 6. ^{59}Co FM-NMR parameters as a function of T for $La_{0.7}Sr_{0.3}CoO_3$ measured in an applied field of 0.5 T: (a) linewidth Δf, (b) spin-spin relaxation rate W_2, and (c) spin-lattice relaxation rate W_1. (The short transverse relaxation time in LSCO prevented measurements for $T>30$ K in this material.)

Korringa-like, the extrapolated $T=0$ K relaxation rate obtained by fitting a line to the data is finite. Measurements at lower T are required to explore this anomalous behavior. In LSMO, the relaxation rate tends to zero in a nonlinear way as $T\rightarrow 0$ K suggesting that magnon processes play a role in relaxation in this temperature range. This is discussed below. Importantly, Fig. 5 shows that with increasing T significant changes in Δf, W_2, and W_1 occur in LSMO above 100 K. The increase in linewidth implies a change in the static hyperfine field distribution due to changes in the electronic structure induced by local lattice distortions. As shown in Fig. 2 with increasing T between 100 and 120 K, the center frequency of the spectrum abruptly shifts downwards by 15 MHz ($\sim$4%). The shift is found to be reversible when T is decreased. There is an accompanying increase in linewidth by a factor 2 between 100 and 120 K followed by a more gradual increase at higher T. For $T>140$ K, the line shape displays structural components and the spectra may be fitted with two Gaussian curves as shown in Fig. 2. For $T>140$ K Savosta and Novak,[29] using ZF NMR, have obtained evidence that phase separation becomes important in both $La_{0.7}Ca_{0.3}MnO_3$ and $La_{0.7}Sr_{0.3}MnO_3$. Two FM components, with somewhat different nuclear spin-spin relaxation rates, were found in these systems. The two coexisting FM phases evolve with T and the less conductive phase is assigned characteristic dimensions in the nanoscale range. The present line shape results are broadly consistent with this model although the low frequency peak appears less pronounced than in the ZF spectra. Possible structural changes inducing the change in the spectra for $T>100$ K are discussed below. The spin-lattice relaxation rate results are discussed in detail in the following sections with emphasis on the low temperature behavior.

C. Low-T relaxation: LSCO

In LSCO the σ^* conduction band electrons are expected primarily to have e_g character, and in Eqs. (2) and (3) we expect $F^{\mathrm{orb}}(\Gamma)<1$. In order to obtain an extreme upper bound value for W_1^{orb}/T for LSCO, we take $F^{\mathrm{orb}}(\Gamma)=1$ (corresponding to equal admixtures of e_g and t_{2g} orbitals), $\langle H_{\mathrm{hf}}^{\mathrm{orb}}\rangle=\mu_B\langle r_{\mathrm{Co}^{3+}}^{-3}\rangle_F$, with $\langle r_{\mathrm{Co}^{3+}}^{-3}\rangle_F=0.4\times 10^{25}$ cm^{-3} (using the radius of the Co^{3+}ion[2]) and for the density of states (DOS) $\rho(E_F)=22.8$ eV/ion from electronic specific heat results.[31](It has been suggested that the bare DOS in NMR relaxation may differ slightly from the specific heat value,[32] but for our estimate we ignore such effects.) For DE systems, we expect the majority spin band to be of primary importance in nuclear relaxation. Approximating $\rho_\uparrow^2(E_F)$ by $\rho^2(E_F)$ (see below) we obtain $^{59}W_1^{\mathrm{orb}}/T=380$ s K^{-1}. The value is in reasonable agreement with the measured value of 300 s K^{-1} obtained from Fig. 4 which suggests that the orbital mechanism makes a dominant contribution to the relaxation process in LSCO. The dipolar contribution W_1^{dip} is an order of magnitude smaller than our upper bound limit for W_1^{orb}.

In evaluating the DOS at the Fermi level, we consider the ratio $P=\rho_\uparrow^2(E_F)/[\rho_\downarrow^2(E_F)+\rho_\uparrow^2(E_F)]$, which gives a measure of the spin polarization. Using available DOS values from LSDA results,[33] we estimate the factor $P>0.8$ for LSCO, corresponding to a much larger DOS in the majority spin band than in the minority spin band, and this permits the approximation $\rho_\uparrow^2(E_F)=\rho^2(E_F)$. To our knowledge no experimental measurements of the spin polarization have been published. Uncertainties in the DOS factor are seen to be small compared to uncertainties in other quantities in Eq. (1). Possible changes in the DOS are linked to changes in disorder.

The present measurements of the transverse relaxation rate confirm previous work,[25] which shows that for LSCO W_2 has a similar T dependence to that shown by W_1, with W_2 roughly an order of magnitude larger than W_1. This suggests that a common mechanism involving hyperfine coupling to carriers in the conduction band is responsible for both longitudinal and transverse relaxation. For isotropic hyperfine fields, we expect $W_2(T)=W_1(T)$.[27] The order-of-magnitude difference in the transverse and longitudinal rates reflects the importance of anisotropic hyperfine effects in this system.

In LSCO, the NMR spectra can be recorded only for $T<30$ K because the short T_2 prevents spin echo signals from being observed at higher T. Over the range 2–30 K, $\Delta f/f_{\mathrm{max}}$ is more than an order of magnitude larger than in LSMO and remains roughly constant. For rhombohedral LSCO static coherent JT distortions do not exist in the metallic state, but dynamic JT effects have been detected using neutron scatter-

ing for $x<0.3$.[17] Local static JT distortions exist in the insulating phase for all x. Neutron scattering has further shown that the transition to the metallic state is accompanied by local distortions of the lattice and a JT glasslike state has been proposed in this region of the phase diagram.[34] With increasing x the lattice tends towards cubic and long-range static JT distortions have been observed in LSCO for $x>0.3$.[34,35] Our previous NMR work has shown that the linewidth from the FM phase is almost independent of x.[8] This points away from local fluctuations in Sr concentration being responsible for the distribution of hyperfine couplings. Local static JT distortions at a fraction of the sites in the FM phase of LSCO give rise to local changes in the electronic structure and anisotropy in the hyperfine coupling. The broad spectral line shape in LSCO is probably linked to these local lattice distortions. In contrast, spectral broadening effects are relatively small in the $x=0.3$ LSMO sample at low T. The LSCO spectra in Fig. 3 can be fit using a Gaussian peak of width $\sim$57 MHz. While the spectrum shows small structural features, it appears that the line shape is primarily due to a broad distribution of hyperfine couplings.

D. Low-T relaxation: LSMO

In the case of LSMO, heat capacity measurements[36] show that $\rho(E_F)$ is sixteen times smaller than in LSCO.[31] This difference may be linked to the increased bandwidth, corresponding to a larger transfer integral t, in LSMO compared to LSCO. Because of the larger splitting of the t_{2g} and e_g states in LSMO compared to LSCO, we expect the mixing factor to be reduced, i.e., $F^{\mathrm{orb}}(\Gamma)^{\mathrm{LSMO}}<F^{\mathrm{orb}}(\Gamma)^{\mathrm{LSCO}}$. For LSMO there is evidence, including point-contact Andreev reflection measurements, that $P>0.8$.[37–39] Recent spin polarized tunneling experiments suggest that the system is close to being a half-metal corresponding to $P\sim 1$.[40] These results for P justify approximating $\rho_{\downarrow}(E_F)$ by $\rho(E_F)$. Equation (1) shows that the combination of the reduced DOS at E_F and a smaller value of $F^{\mathrm{orb}}(\Gamma)$, because of a reduced t_{2g} admixture, leads to a large reduction in the orbital contribution to relaxation compared to LSCO. We obtain the following estimate ${}^{55}W_1^{\mathrm{orb}}/T=1.2\ \mathrm{s\ K^{-1}}$ as an upper limit with a lower limit at least an order of magnitude smaller. This is to be compared with the experimental value ${}^{55}W_1^{\mathrm{orb}}\sim 0.3\ \mathrm{s^{-1}}$ at 2 K. While the estimate shows that the orbital process can make a contribution to relaxation at low temperatures, the experimental results suggest that other relaxation mechanisms, specifically spin waves, are dominant in LSMO leading to the nonlinear temperature dependence of ${}^{55}W_1$ for $T<70$ K. The heat capacity measurements have shown that conventional spin waves, with no gap, are present in this system.[36,41] While the conduction band hyperfine mechanism is not dominant at low T, this mechanism appears to become increasingly important for T above 100 K. The LSMO data can be fit over the range 10–100 K using the two-magnon relaxation expression given in Eq. (5) written in the form ${}^{55}W_1^{\mathrm{magnon}}=C_m\ln(k_BT/g\mu_BSH)T^2$. The least squares fit to the 3 T results is shown in the inset in Fig. 4 and gives $C_m=8.6\times10^{-3}\pm0.5\times10^{-3}\ \mathrm{s^{-1}\ K^{-2}}$. From experiment the hyperfine coupling is $A/\hbar\sim 2.3\times10^9\ \mathrm{s^{-1}}$ and the spin wave stiffness constant is[36,41] $D=2JSa^2=180\ \mathrm{meV\ \AA^2}$ with the lattice spacing $a=3.9$ Å. Inserting these values into the theoretical expression $C_m=A^2(\sin^2\alpha)k_B^2\hbar/\hbar^2 2(2\pi)^3(2JS)^3$ gives $C_m=3.0\times10^{-2}\sin^2\alpha\ \mathrm{s^{-1}\ K^{-2}}$. At low T, where JT effects are not important, we expect the hyperfine anisotropy angle α to be small and the factor $\sin^2\alpha$ will reduce the theoretical value by one to two orders of magnitude. Agreement between the theoretical estimate and the experimental value for C_m is therefore roughly within an order of magnitude, and we conclude that spin wave relaxation is the likely relaxation mechanism in the low temperature range where the carrier scattering mechanism is not of primary importance. Changes in the hyperfine anisotropy, caused by JT distortions, result in changes in electronic structure and hence in nuclear relaxation. This can be seen using simple arguments based on the fluctuating transverse hyperfine field amplitude. In examining changes in relaxation behavior with T for LSMO, it is of interest to consider the behavior of W_2. Tracking behavior of W_2 with W_1 has been found in $La_{1-x}Na_xMnO_3$ for $T>70$ K.[24] The present results indicate that W_1 is increasing with T in a similar way to W_2 as the temperature approaches 200 K. For $T<70$ K in LSMO, W_2 no longer tracks W_1 suggesting that a different mechanism, such as the Suhl-Nakamura virtual magnon process,[18] has become important in spin-spin-relaxation in this range in agreement with previous NMR experiments.[29]

E. Relaxation at higher T: LSMO

The likely source of thermally-induced changes in relaxation behavior is static JT distortion of the oxygen octahedra, which lowers the symmetry at a significant fraction of the ^{55}Mn sites resulting in a distribution of anisotropic hyperfine couplings. Evidence for the suggested importance of changes in the anisotropic interactions can be obtained from the behavior of the NMR spectra with T. Figures 5(a) and 6(a) show the linewidths Δf as a function of T for the two systems. In LSMO, Δf in an applied field of 3 T initially remains almost constant as T is increased up to 100 K but increases significantly for $T>120$ K. This is linked to the splitting of the line into two FM components as discussed above. There is an accompanying increase in the relaxation rates. It is interesting to note that these increases occur over the temperature range in which the resistivity, shown in Fig. 1, increases by almost an order of magnitude. This suggests that a common mechanism, specifically JT distortions in the lattice, is of dominant importance in determining this behavior.[42,43] The increase in W_1 can be understood using the phenomenological Eqs. (9) and (11) as resulting from changes in the HF anisotropy and in the DE correlation time τ produced by JT distortions. It appears that W_1 approaches W_2 with increasing T as predicted for the electron scattering mechanism that becomes of dominant importance at the highest temperatures shown. For localized electron systems, estimates of the Mn^{3+} anisotropic dipolar hyperfine field due to JT distortion, and the resultant changes in the ground state wave function, give values that are a significant fraction of the isotropic field[44] and somewhat larger than the $\sim$4% frequency shifts observed around 120 K for mixed valence me-

tallic LSMO in the present experiments. It appears that, in contrast to LSCO for which conduction electron scattering is of dominant importance in ^{59}Co relaxation at all T for which signals are observed, ^{55}Mn relaxation in LSMO involves electron scattering as the dominant mechanism only for $T > T_c/3$. It is interesting to note that the temperature range over which marked changes in linewidth and relaxation rates occur for LSMO roughly coincides with the range 100–200 K in which the resistivity increases rapidly. Recent EXAFS measurements suggest a gradual change in the average Mn-O bond length with T below T_c (Ref. 45), whereas the present measurements are consistent with JT distortions becoming increasingly important for $T > T_c/3$. This is consistent with JT-induced disorder being the underlying mechanism for both effects in this temperature range.

CONCLUSION

NMR spectral line shape and relaxation rate measurements in DE ferromagnets LSMO and LSCO (with $x=0.3$) made as a function of T in the FM phase show marked differences in behavior of the two systems. The relaxation rate results are analyzed using theoretical expressions for conduction band electron hyperfine couplings involving an orbital mechanism. In LSCO, it is concluded that the carrier scattering mechanism plays an important role in ^{59}Co relaxation over the temperature range 2–30 K for which FM NMR measurements could be made. In LSMO, the results show that anisotropic hyperfine couplings become important for $T > 120$ K. The observed changes are reversible with T and are consistent with cooperative JT distortions. The differences in behavior of the systems with temperature are attributed to differences in DE couplings, and in JT-induced lattice disorder. For $T < 100$ K ^{55}Mn spin-lattice relaxation in LSMO involves a two-magnon process with measured relaxation rates much smaller than in LSCO.

The contrasting behavior of the two systems is attributed to differences in DE couplings, which are larger in LSMO than in LSCO, and in the relative importance of JT distortions in the two systems. The results show that a major difference between metallic LSCO and LSMO is the enhanced importance of low-temperature local lattice distortions in LSCO compared to LSMO. It is only for $T > 100$ K in LSMO that local JT distortions "kick in," as revealed by the FM-NMR results, leading to changes in the transport and magnetic properties. Theoretical models for LSMO and LSCO should reflect the different roles that disorder plays in these two systems.

ACKNOWLEDGMENTS

Financial support by the NSF under Cooperative Agreement No. DMR 0084173 and by the State of Florida is gratefully acknowledged. Work at UMN was supported by DOE (Grant No. DE-FG02-06ER46275), NSF (Grant No. DMR-0509666) and the ACS PRF.

[1] *Colossal Magnetoresistance Oxides*, edited by Y. Tokura (Gordon and Breach, New York, 2000).
[2] J. M. D. Coey, M. Viret, and S. von Molnar, Adv. Phys. **48**, 167 (1999).
[3] M. B. Salamon and M. Jaime, Rev. Mod. Phys. **73**, 583 (2002).
[4] E. Dagotto, *Nanoscale Phase Separation and Colossal Magnetoresistance*, Vol. 136 of *Springer Series in Solid Sate Sciences* (Springer, Berlin, 2002).
[5] R. Caciuffo, D. Rinaldi, G. Barucca, J. Mira, J. Rivas, M. A. Sĕnarís-Rodríguez, P. G. Radaelli, D. Fiorani, and J. B. Goodenough, Phys. Rev. B **59**, 1068 (1999).
[6] J. Mira, J. Rivas, G. Baio, G. Barucca, R. Caciuffo, D. Rinaldi, D. Fiorani, and M. A. Sĕnarís-Rodríguez, J. Appl. Phys. **89**, 5606 (2001).
[7] J. Wu and C. Leighton, Phys. Rev. B **67**, 174408 (2003).
[8] P. L. Kuhns, M. J. R. Hoch, W. G. Moulton, A. P. Reyes, J. Wu, and C. Leighton, Phys. Rev. Lett. **91**, 127202 (2003).
[9] C. Zener, Phys. Rev. **82**, 403 (1951).
[10] P. W. Anderson and H. Hasegawa, Phys. Rev. **100**, 675 (1955).
[11] P.-G. de Gennes, Phys. Rev. **118**, 141 (1960).
[12] J. Burgy, A. Moreo, and E. Dagotto, Phys. Rev. Lett. **92**, 097202 (2004).
[13] K. H. Ahn, T. Lookman, and A. R. Bishop, Nature (London) **428**, 401 (2004).
[14] G. C. Milward, M. J. Calderón, and P. B. Littlewood, Nature (London) **433**, 607 (2005).
[15] A. P. Ramirez, J. Phys.: Condens. Matter **9**, 8171 (1997).
[16] M. A. Korotin, S. Yu. Ezhov, I. V. Solovyev, V. I. Anisimov, D. I. Khomskii, and G. A. Sawatzky, Phys. Rev. B **54**, 5309 (1996); P. M. Raccah and J. B. Goodenough, Phys. Rev. **155**, 932 (1967).
[17] D. Louca and J. L. Sarrao, Phys. Rev. Lett. **91**, 155501 (2003).
[18] H. M. Aarbogh, J. Wu, L. Wang, H. Zheng, J. F. Mitchell, and C. Leighton, Phys. Rev. B **74**, 134408 (2006).
[19] Y. Obata, J. Phys. Soc. Jpn. **18**, 1020 (1963).
[20] T. Moriya, J. Phys. Soc. Jpn. **19**, 681 (1964).
[21] Y. Yafet and V. Jaccarino, Phys. Rev. **133**, A1630 (1964).
[22] A. H. Mitchell, J. Chem. Phys. **27**, 17 (1957).
[23] D. Beeman and P. Pincus, Phys. Rev. **166**, 359 (1968).
[24] M. M. Savosta, V. A. Borodin, and P. Novák, Phys. Rev. B **59**, 8778 (1999).
[25] M. J. R. Hoch, P. L. Kuhns, W. G. Moulton, A. P. Reyes, J. Wu, and C. Leighton, Phys. Rev. B **69**, 014425 (2004).
[26] A. Abragam, *The Principles of Nuclear Magnetism* (Oxford University Press, Oxford, 1961).
[27] E. A. Turov and M. P. Petrov, *Nuclear Magnetic Resonance in Ferro- and Antiferromagnets* (Halsted Press, New York, 1972).
[28] A. Urushibara, Y. Moritomo, T. Arima, A. Asamitsu, G. Kido, and Y. Tokura, Phys. Rev. B **51**, 14103 (1995).
[29] M. M. Savosta and P. Novák, Phys. Rev. Lett. **87**, 137204 (2001).
[30] M. Itoh and I. Natori, J. Phys. Soc. Jpn. **64**, 970 (1995).
[31] M. Paraskevopoulos, J. Hemberger, A. Krimmel, and A. Loidl, Phys. Rev. B **63**, 224416 (2001).
[32] A. Narath, in *Hyperfine Interactions*, edited by A. J. Freeman and

R. B. Frankel (Academic Press, New York, 1967).
[33] P. Ravindran, H. Fjellvåg, A. Kjekshus, P. Blaha, K. Schwarz, and J. Luitz, J. Appl. Phys. **91**, 291 (2002).
[34] D. Louca, J. L. Sarrao, J. D. Thompson, H. Röder, and G. H. Kwei, Phys. Rev. B **60**, 10378 (1999).
[35] D. Phelan, D. Louca, S. Rosenkranz, S.-H Lee, Y. Qiu, P. J. Chupas, R. Osborn, H. Zheng, J. F. Mitchell, J. R. D. Copley, J. L. Sarrao, and Y. Moritomo, Phys. Rev. Lett. **96**, 027201 (2006).
[36] B. F. Woodfield, M. L. Wilson, and J. M. Byers, Phys. Rev. Lett. **78**, 3201 (1997).
[37] W. E. Pickett and D. J. Singh, Phys. Rev. B **53**, 1146 (1996).
[38] B. Nadgorny, I. I. Mazin, M. Osofsky, R. J. Soulen, Jr., P. Broussard, R. M. Stroud, D. J. Singh, V. G. Harris, A. Arsenov, and Ya. Mukovskii, Phys. Rev. B **63**, 184433 (2001).
[39] Y. Ji, C. L. Chien, Y. Tomioka, and Y. Tokura, Phys. Rev. B **66**, 012410 (2002).
[40] M. Bowen, M. Bibes, A. Barthélémy, J.-P. Contour, A. Anane, Y. Lemaître, and A. Fert, Appl. Phys. Lett. **82**, 233 (2003); M. Bowen, A. Barthélémy, M. Bibes, E. Jacquet, J. P. Contour, A. Fert, D. Wortmann, and S. Blügel, J. Phys.: Condens. Matter **17**, L407 (2005).
[41] A. H. Moudden, L. Vasiliu-Doloc, L. Pinsard, and A. Revcolevschi, Physica B **241-243**, 276 (1998).
[42] A. J. Millis, P. B. Littlewood, and B. I. Shraiman, Phys. Rev. Lett. **74**, 5144 (1995).
[43] D. Louca and T. Egami, Phys. Rev. B **59**, 6193 (1999).
[44] T. Kubo, T. Goto, T. Koshiba, K. Takeda, and K. Awaga, Phys. Rev. B **65**, 224425 (2002).
[45] L. Downward, F. Bridges, S. Bushart, J. Neumeier, N. Dilley, and L. Zhou, Phys. Rev. Lett. **95**, 106401 (2005).